# Topology optimization of sound absorbing layer for the mid-frequency vibration of vibro-acoustic systems

Ruxin Gao[a], Yahui Zhang[a*], David Kennedy[b]

[a] *State Key Laboratory of Structural Analysis for Industrial Equipment, Department of Engineering Mechanics, International Center for Computational Mechanics, Dalian University of Technology, Dalian 116023, PR China;*

[b] *School of Engineering, Cardiff University, Cardiff CF24 3AA, Wales, UK*

Corresponding author:

Dr. Y. H. Zhang

State Key Laboratory of Structural Analysis for Industrial Equipment, Department of Engineering Mechanics, Dalian University of Technology, Dalian 116023, PR China

Email: zhangyh@dlut.edu.cn

Tel: +86 411 84706337

Fax: +86 411 84708393

# Abstract

Due to the significant difference of dynamic properties between the fluid medium and the structure, when a vibro-acoustic system is subjected to a higher frequency excitation, it may typically exhibit mid-frequency behavior which involves different wavelength deformations and is very sensitive to the uncertainties of the system. This paper deals with optimized distribution of a sound absorbing layer for the mid-frequency vibration of vibro-acoustic systems by using hybrid boundary element analysis and statistical energy analysis. Based on the SIMP approach an artificial sound absorbing material model is suggested and the relative densities of the sound absorbing material are taken as design variables. The sound pressure level at a specified point in the acoustic cavity is to be minimized by distributing a given amount of sound absorbing material. An efficient direct differentiation scheme for the response sensitivity analysis is proposed. Then the optimization problem is solved by using the method of moving asymptotes. A numerical example illustrates the validity and effectiveness of the present optimization model. Impact of the excitation frequency on optimized topology is also discussed.



**Keywords**: Mid-frequency; Vibro-acoustic system; Sound absorbing layer; Boundary element; Statistical energy analysis; Dynamic topology optimization

# 1 Introduction

Vibro-acoustic systems are widely used in vehicles such as automobiles, trains, ships and rocket launchers. These vehicles may be subjected to complex environmental excitations during their operation, resulting in strong structural vibration and harmful high noise levels. Early studies on vibration and noise control (see e.g. Christensen et al. 1998a, b) mainly alter the shape and size of system components to control the generation of noise at the sound source. With the development of topology optimization techniques (Sigmund 2001; Bendsøe and Sigmund 2003), more and more researchers began to study the noise control problem of vibro-acoustic systems by using topology optimization techniques. Yoon et al. (2007) dealt with the problem of topology optimization of vibro-acoustic systems using a mixed finite element (FE) formulation (Zienkiewicz and Taylor 2000; Bathe 2008), in which the acoustic cavity is enclosed by a finite boundary. Kook et al. (2012) proposed a design method for acoustical topology optimization considering human hearing characteristics. Shu et al. (2014) studied the topology optimization of vibro-acoustic systems for minimizing sound pressure by using the level set method. To date, the studies on topology optimization of vibro-acoustic systems have been mainly focused on the optimized distribution of structural materials, while the topology optimization of damping or sound absorbing layers has been rarely involved.

However, the design of a large vehicle should not only consider vibration and noise reduction, but also meet other design requirements including stiffness, strength, stability,

aerodynamics and hydrodynamics. Therefore, design methods for vibration and noise reduction by finding the optimized layout of structural material have some limitations. At present, a commonly used method is to place damping material on the surface of a structure and sound absorbing material on the sound propagation path to reduce the acoustic radiation and the reflection or transmission of sound waves, respectively. However, a large area of damping or sound absorbing material will cause a sharp increase in system weight, which will not only affect the system performance but also increase the manufacturing cost. In view of the above situation, topology optimization techniques are used to obtain the optimized layout of damping or sound absorbing layers in a vibro-acoustic system. Dühring et al. (2008) studied the optimized placement of damping panels on walls of acoustic cavities by using the solid isotropic material with penalization (SIMP) method (Sigmund 2001; Bendsøe and Sigmund 2003). The sound level can be significantly reduced by optimizing the distribution of the sound absorbing and reflecting material. Akl et al. (2009) developed a mathematical model to simulate fluid-structure interactions based on FE method. A good agreement was obtained between the results obtained from the mathematical model and those from the experiment. Zhang and Kang (2013) presented a topology optimization model to obtain the optimized layout of a damping layer for minimizing the acoustic radiation of damped thin-walled structures. In their paper, the dynamic coupling between the acoustic medium and the structure is neglected. Then considering the velocity response of the structure which is calculated by

FE method as an acoustic excitation, the sound pressure at a reference point is obtained by using the boundary element (BE) method (Ciskowski and Brebbia 1991; Wu 2000). They also proposed a sensitivity analysis scheme using the adjoint variable method. Zhao et al. (2017) studied the optimized design of sound absorbing material distribution within sound barrier structures based on the BE method and the optimality criteria method. A smoothed Heaviside-like function was developed to help the SIMP method to obtain a clear 0-1 distribution. The optimized distribution of the sound absorbing material is strongly frequency dependent according to the results obtained by authors, and the optimization in a frequency band was suggested. Du and Olhoff (2007, 2010) studied the topology optimization problem of vibrating bi-material elastic structures placed in an acoustic medium for minimizing the acoustic radiation and gave a corresponding sensitivity analysis scheme. Their papers assumed that the vibration frequency of a structure has a sufficiently high value, so that the radiation impedance at the structure boundary is approximately equal to the characteristic impedance of the acoustic medium (Lax and Feshbach 1947; Herrin et al. 2003). Thus the sound pressure in the acoustic field can be easily obtained by using a high frequency boundary integral equation. Considering that resonance and wave-propagation problems are known to be highly sensitive towards parameter variations and the conventional robust topology optimization methods for structural problems are not suitable for the acoustic problem, Christiansen et al. (2015) suggested a new double filter approach and obtained highly robust designs for acoustic

problem. Christiansen and Sigmund (2015) provide the experimental validation of an acoustic cavity designed using topology optimization with the goal of minimizing the sound pressure locally for monochromatic excitation.

Based on deterministic methods, such as the FE method, several of the papers mentioned above studied the topology optimization of vibro-acoustic systems. As the frequency increases, the deformation wavelength of the system components will decrease significantly. A fine mesh is required to capture the detailed deformation, typically six to eight elements per wavelength (Simmons 1991; Steel and Craik 1994), which leads to a large number of degrees of freedom (DOF). The computational cost of element-based techniques typically increases due to decreasing wavelengths and multiple reanalyses in the optimization process (Cotoni et al. 2007). Moreover, as the frequency increases, the response of a system will be more and more sensitive to the uncertainties which are inevitably generated during the manufacturing process. Systems with the same nominal geometric and material parameters may produce different responses. At this point, it makes no sense to analyze only one system, and an estimate of average behavior of an ensemble of similar systems with the same nominal properties might be preferred (Ladeveze et al. 2012). As a common statistical method, statistical energy analysis (SEA) (Lyon and DeJong 1995), can give an average prediction for the statistical behavior of systems with little computational cost. However, the assumptions introduced in SEA can only be satisfied when the system is subjected to sufficiently high frequencies (Lyon and

DeJong 1995; Langley 1989a). In addition, based on SEA the properties of a system may be highly generalized as some parameters are independent of the material topology layout, which makes topology optimization impossible.

Due to the significant difference of dynamic properties between the fluid medium and the structure, when a vibro-acoustic system is subjected to a higher frequency excitation, it may typically exhibit mid-frequency behavior in which some subsystems are large compared with a wavelength, while others are small compared with a wavelength (Shorter and Langley 2005b). At present, neither the FE method nor SEA can describe the motion of vibro-acoustic systems well. To address this situation, three types of improved methods have been proposed for the mid-frequency vibration of complex systems. The first type aims to extend the effective frequency range of traditional deterministic methods to the mid-frequency domain (see e.g. Langley 1989b; Van Vinckenroy and De Wilde 1995; Harari and Avraham 1997; Pluymers et al. 2007; Hinke et al. 2009; Ma et al. 2015b). The second type aims to relax the assumptions in SEA to extend its application to the mid-frequency domain (see e.g. Keane and Price 1987; Langley 1992; Maxit and Guyader 2003; Mace 2005). The third type combines the deterministic and statistical methods to develop a hybrid model for the mid-frequency vibration of complex systems (see e.g. Zhao and Vlahopoulos 2000; Shorter and Langley 2005a, b; Ji et al. 2006; Vergote et al. 2011; Zhu et al. 2014; Ma et al. 2015a; Gao et al. 2018). As the most popular hybrid approach, the hybrid FE-SEA method proposed by

Shorter and Langley (2005b) divides a complex system into a number of deterministic and statistical subsystems according to the deformation wavelength. The so-called deterministic subsystem which is subjected to long wavelength deformation can be modeled by using the FE method, while the so-called statistical subsystem which is subjected to short wavelength deformation can be modeled by using SEA. The dynamic coupling between the two types of subsystems is described as the reflection and transmission of the vibration wave. Based on the diffuse field reciprocity principle (Shorter and Langley 2005a), a non-iterative relationship between the deterministic and statistical subsystems can be established. Due to the combination of the FE method and SEA, the hybrid FE-SEA method can give an average prediction for the mid-frequency vibration and deal with actual engineering systems. Considering the BE method to describe the motion of an acoustic cavity, Gao et al. (2018) proposed the hybrid BE-SEA method for the mid-frequency vibration of vibro-acoustic systems. Due to the nature of the BE method, the hybrid BE-SEA method not only satisfies the Sommerfeld radiation condition at infinity for exterior acoustic problem, but is also more efficient in the modeling stage. Since hybrid approaches are more appropriate than the traditional method for the mid-frequency of complex systems, Muthalif and Langley(2012) studied the active control of mid-frequency vibration by using the hybrid FE-SEA method as an analysis tool. The optimized skyhook damping value and its location were calculated by using the MATLAB GADS toolbox with combined pattern search and genetic algorithms. By using

the hybrid FE-wave based (WB) method, Goo et al. (2017) proposed an efficient topology optimization method for bounded acoustic problems. Their method employs the FE method and WB method to respectively model the design and non-design domains to increase computational efficiency and can thus be applied to higher frequency applications that conventional method takes considerable computation time to manage.

The present work studies optimized distribution of a sound absorbing layer for the mid-frequency vibration of vibro-acoustic systems by using the hybrid BE-SEA method. In the topology optimization model, an artificial sound absorbing material model is established by employing the SIMP approach. The design objective is the sound pressure level at a specified point in the acoustic cavity, and the design variables are the relative densities of the sound absorbing material. The corresponding sensitivity analysis scheme is derived by direct differentiation. The basic principles of the hybrid BE-SEA method are outlined in Section 2. The topology optimization problem formulation and the corresponding sensitivity analysis scheme are developed in Section 3. In Section 4, a numerical example is presented to illustrate the efficiency of the hybrid BE-SEA method and the validity of the proposed topology optimization model. The impact of the excitation frequency on optimized topology is also discussed. Finally, conclusions are given in Section 5.

# 2 Basic principles of hybrid BE-SEA method

The hybrid BE-SEA method was proposed by Gao et al. (2018) for the mid-frequency vibration of vibro-acoustic systems based on the concept of the hybrid FE-SEA method. Due to the use of the BE method, the hybrid BE-SEA method provided an appropriate model with modeling advantages when the deterministic part of the model is a relatively large acoustic domain.

Without loss of generality, this section demonstrates the basic principles of the hybrid BE-SEA method. In a vibro-acoustic system, the fluid is confined in a bounded acoustic domain $\Omega$, as shown in Fig. 1, of which the boundary surface $\Gamma_a$ contains a velocity surface $\Gamma_v$, an impedance (sound absorbing) surface $\Gamma_Z$ and an elastic thin-walled structural surface $\Gamma_s$. The velocity and impedance boundary conditions are expressed by a generalized equation which can be written as (Wu 2000)

$$\mathbf{v}_{\mathrm{n}} = \mathbf{C}_\beta \mathbf{C}_\gamma - \mathbf{C}_\beta \mathbf{C}_\alpha \mathbf{p} \tag{1}$$

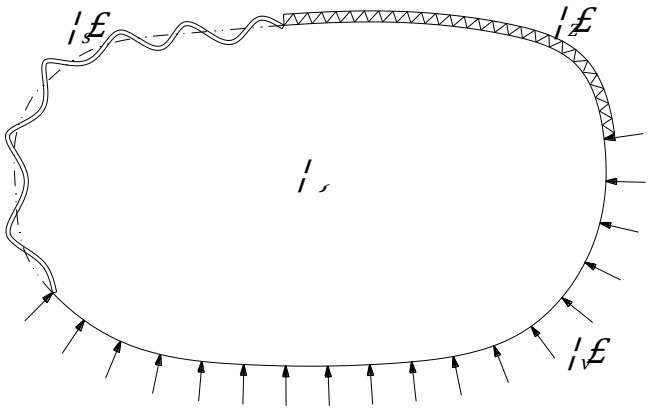

Fig. 1 Coupled vibro-acoustic system. $\Omega$, acoustic domain; $\Gamma_v$, velocity boundary surface; $\Gamma_Z$, impedance boundary surface; $\Gamma_s$, elastic thin-structural surface.

where the vectors $\mathbf{p}$ and $\mathbf{v}_{\mathrm{n}}$ respectively represent the sound pressures and normal velocities at nodal points on the boundary of the acoustic cavity. $\mathbf{C}_{\alpha}$ and $\mathbf{C}_{\beta}$ are constraint coefficient diagonal matrices corresponding to sound pressure and normal velocity, respectively. $\mathbf{C}_{\gamma}$ is a constraint coefficient vector. The hybrid BE-SEA method (Gao et al. 2018) may be employed for the mid-frequency vibration of the system. The acoustic cavity modeled by the BE method is treated as the deterministic subsystem, while the thin-walled structure modeled by SEA is treated as the statistical subsystem. According to the hybrid BE-SEA method, the response of the statistical thin-walled structure is viewed as the superposition of the direct and reverberant fields (see Shorter and Langley 2005a). Considering the velocity and impedance boundary conditions and the coupling interaction between the acoustic cavity and the direct field of the thin-walled structure, the governing equation of the system can be written as (Gao et al. 2018)

$$\begin{bmatrix} \widetilde{\mathbf{H}} & -\mathrm{i}\omega\mathbf{G}\mathbf{T} \\ -\mathbf{A} & \mathbf{D}_{\mathrm{dir}} \end{bmatrix} \begin{Bmatrix} \mathbf{p} \\ \mathbf{u} \end{Bmatrix} = \begin{Bmatrix} \mathbf{G}\bar{\mathbf{v}}_{\mathrm{n}} \\ \mathbf{0} \end{Bmatrix} + \begin{Bmatrix} \mathbf{0} \\ \mathbf{f}_{\mathrm{rev}}^{\mathrm{s}} \end{Bmatrix} \tag{2}$$

where $\bar{\mathbf{v}}_{\mathrm{n}} = \mathbf{C}_{\beta}\mathbf{C}_{\gamma}$, $\widetilde{\mathbf{H}} = \mathbf{H} + \mathbf{G}\mathbf{C}_{\beta}\mathbf{C}_{\alpha}$, $\mathbf{H}$ and $\mathbf{G}$ are the influence matrices of sound pressure and normal velocity, respectively. $\mathbf{D}_{\mathrm{dir}}$ and $\mathbf{u}$ are the dynamic stiffness matrix and displacement vector of the direct field of the thin-walled structure, respectively. $\mathbf{f}_{\mathrm{rev}}^{\mathrm{s}}$ is the vector of the blocked reverberant forces. $\mathbf{A}$ is a coupling coefficient matrix which converts the sound pressure vector of the acoustic cavity into the nodal force vector of the direct field of the thin-walled structure. $\mathbf{T}$ is the transformation matrix resulting from

the non-conforming grids appearing at the fluid-structure coupling face, $\omega$ is the angular frequency, and $\mathrm{i} = \sqrt{-1}$. For the sake of simplicity, Equation (2) will be written as

$$\mathbf{D}_{\mathrm{tot}}\mathbf{q} = \mathbf{f}_{\mathrm{ext}} + \mathbf{f}_{\mathrm{rev}} \tag{3}$$

where $\mathbf{D}_{\mathrm{tot}} = \begin{bmatrix} \widetilde{\mathbf{H}} & -\mathrm{i}\omega\mathbf{G}\mathbf{T} \\ -\mathbf{A} & \mathbf{D}_{\mathrm{dir}} \end{bmatrix}$ and $\mathbf{q} = \begin{Bmatrix} \mathbf{p} \\ \mathbf{u} \end{Bmatrix}$ respectively represent the total dynamic stiffness matrix and the vector of all deterministic DOF. $\mathbf{f}_{\mathrm{ext}} = \begin{Bmatrix} \mathbf{G}\bar{\mathbf{v}}_{\mathrm{n}} \\ \mathbf{0} \end{Bmatrix}$ and $\mathbf{f}_{\mathrm{rev}} = \begin{Bmatrix} \mathbf{0} \\ \mathbf{f}_{\mathrm{rev}}^{\mathrm{s}} \end{Bmatrix}$ respectively represent the vectors of all external and blocked reverberant forces.

If there is sufficient uncertainty in the statistical subsystem, the statistics of the blocked reverberant force tend to zero (see Shorter and Langley 2005a). Rewriting equation (3) in cross-spectral form and averaging over an ensemble of statistical thin-walled structures gives

$$\mathbf{S}_{qq} = \langle \mathbf{q}\mathbf{q}^{\mathrm{H}} \rangle = \begin{bmatrix} \mathbf{S}_{pp} & \mathbf{S}_{pu} \\ \mathbf{S}_{up} & \mathbf{S}_{uu} \end{bmatrix} = \mathbf{S}_{qq}^{\mathrm{ext}} + \mathbf{S}_{qq}^{\mathrm{rev}} \tag{4}$$

where $\mathbf{S}_{qq}$ represents the cross-spectrum matrix of the deterministic DOF. $\#^{\mathrm{H}}$ is the Hermitian transpose of $\#$, and $\langle \# \rangle$ is the ensemble average of $\#$. The subscripts $p$ and $u$ stand for the DOF of the acoustic cavity and the direct field of the thin-walled structure. Also

$$\mathbf{S}_{qq}^{\mathrm{ext}} = \mathbf{D}_{\mathrm{tot}}^{-1}\mathbf{S}_{ff}^{\mathrm{ext}}\mathbf{D}_{\mathrm{tot}}^{-\mathrm{H}} = \begin{bmatrix} \mathbf{S}_{pp}^{\mathrm{ext}} & \mathbf{S}_{pu}^{\mathrm{ext}} \\ \mathbf{S}_{up}^{\mathrm{ext}} & \mathbf{S}_{uu}^{\mathrm{ext}} \end{bmatrix} \tag{5}$$

$$\mathbf{S}_{qq}^{\mathrm{rev}} = \mathbf{D}_{\mathrm{tot}}^{-1}\mathbf{S}_{ff}^{\mathrm{rev}}\mathbf{D}_{\mathrm{tot}}^{-\mathrm{H}} = \begin{bmatrix} \mathbf{S}_{pp}^{\mathrm{rev}} & \mathbf{S}_{pu}^{\mathrm{rev}} \\ \mathbf{S}_{up}^{\mathrm{rev}} & \mathbf{S}_{uu}^{\mathrm{rev}} \end{bmatrix} \tag{6}$$

where $\mathbf{S}_{ff}^{\mathrm{ext}} = \langle \mathbf{f}_{\mathrm{ext}} {\mathbf{f}_{\mathrm{ext}}}^{\mathrm{H}} \rangle$ and $\mathbf{S}_{ff}^{\mathrm{rev}} = \langle \mathbf{f}_{\mathrm{rev}} {\mathbf{f}_{\mathrm{rev}}}^{\mathrm{H}} \rangle$ respectively represent the cross-spectrum matrices of the total external and blocked reverberant forces. $\#^{-\mathrm{H}}$ represents the Hermitian transpose of the inverse matrix. Considering the diffuse field reciprocity principle (see Shorter and Langley 2005a), equation (6) can be rewritten in terms of the reverberant field energy $E$ and the modal density $n_{\mathrm{m}}$ of the thin-walled structure as

$$\mathbf{S}_{qq}^{\mathrm{rev}} = \frac{E}{n_{\mathrm{m}}} \frac{4}{\pi\omega} \boldsymbol{\Upsilon} \tag{7}$$

where

$$\boldsymbol{\Upsilon} = \mathbf{D}_{\mathrm{tot}}^{-1} \mathrm{Im}\{\widetilde{\mathbf{D}}_{\mathrm{dir}}\} \mathbf{D}_{\mathrm{tot}}^{-\mathrm{H}} = \begin{bmatrix} \boldsymbol{\Upsilon}_{pp} & \boldsymbol{\Upsilon}_{pu} \\ \boldsymbol{\Upsilon}_{up} & \boldsymbol{\Upsilon}_{uu} \end{bmatrix} \tag{8}$$

with

$$\widetilde{\mathbf{D}}_{\mathrm{dir}} = \begin{bmatrix} \mathbf{0} & \mathbf{0} \\ \mathbf{0} & \mathbf{D}_{\mathrm{dir}} \end{bmatrix} \tag{9}$$

The cross-spectrum matrix of the deterministic DOF $\mathbf{S}_{qq}$ can be obtained by using equations (4)-(9). The only unknown quantity $E$, at this time, can be calculated by employing the power balance equation of the reverberant field of the thin-walled structure, which is given by (see Gao et al. 2018)

$$(h_{\mathrm{out}}^{\mathrm{rev}} + h_{\mathrm{diss}}) \frac{E}{n_{\mathrm{m}}} = P_{\mathrm{in}} \tag{10}$$

Here, $h_{\mathrm{out}}^{\mathrm{rev}}$ and $h_{\mathrm{diss}}$ respectively represent the total energy leaving the reverberant

field of the thin-walled structure into the acoustic cavity and the total energy dissipating by the damping of the thin-walled structure per unit modal energy density in the reverberant field of the thin-walled structure. $P_{\mathrm{in}} = P_{\mathrm{in}}^{\mathrm{dir}} + P_{\mathrm{in}}^{\mathrm{ext}}$ is the total power input to the statistical thin-walled structure, where $P_{\mathrm{in}}^{\mathrm{dir}}$ is the power arising from the force applied to the acoustic cavity and $P_{\mathrm{in}}^{\mathrm{ext}}$ is the power caused by other sources applied directly to the statistical thin-walled structure. The above parameters can be expressed as

$$P_{\mathrm{in}}^{\mathrm{dir}} = \frac{\omega}{2}\sum_{ij}\mathrm{Im}\{\mathbf{D}_{\mathrm{dir},ij}\}(\mathbf{S}_{uu}^{\mathrm{ext}})_{ij} \tag{11}$$

$$h_{\mathrm{diss}} = \omega n_{\mathrm{m}}\eta \tag{12}$$

$$h_{\mathrm{out}}^{\mathrm{rev}} = \frac{2}{\pi}\mathrm{Re}\left\{-\mathrm{i}\sum_{ij}\mathbf{C}_{\mathrm{sa},ij}\left(\boldsymbol{\Upsilon}_{up}\right)_{ij}^{*}\right\} \tag{13}$$

where $\eta$ is the damping loss factor of the thin-walled structure, $\mathbf{C}_{\mathrm{sa}}$ is a coupling coefficient matrix which connects the shape functions of the grids of the acoustic cavity and the direct field of the thin-walled structure (see Gao et al. 2018). $\#^{*}$ stands for the complex conjugate of $\#$.

By substituting equations (11)-(13) into equation (10), the ensemble average energy of the reverberant field can be obtained. The energy of the direct field of the thin-walled structure can be neglected (see Shorter and Langley 2005b). Hence, by using equations (4)-(9), $\mathbf{S}_{qq}$ can be calculated. Selecting some points inside the acoustic cavity and

calculating the corresponding coefficient matrices $\mathbf{g}$ of sound pressure and $\mathbf{h}$ of normal velocity, the cross-spectrum matrix of sound pressure at these points can be expressed as (see Gao et al. 2018)

$$\mathbf{S}_{pp}^{\mathrm{in}} = \omega^2(\mathbf{g}\mathbf{T}\mathbf{S}_{uu}\mathbf{T}^{\mathrm{H}}\mathbf{g}^{\mathrm{H}}) + \mathrm{i}\omega(\boldsymbol{\Delta} - \boldsymbol{\Delta}^{\mathrm{H}}) + \boldsymbol{\Xi} - \boldsymbol{\Pi} - \boldsymbol{\Pi}^{\mathrm{H}} \tag{14}$$

where

$$\boldsymbol{\Delta} = \mathbf{g}\mathbf{Q}\mathbf{g}^{\mathrm{H}} + \tilde{\mathbf{h}}\mathbf{S}_{pu}\mathbf{T}^{\mathrm{H}}\mathbf{g}^{\mathrm{H}} \tag{15}$$

$$\boldsymbol{\Xi} = \mathbf{g}\mathbf{S}_{\bar{v}_{\mathrm{n}}\bar{v}_{\mathrm{n}}}\mathbf{g}^{\mathrm{H}} + \tilde{\mathbf{h}}\mathbf{S}_{pp}\tilde{\mathbf{h}}^{\mathrm{H}} \tag{16}$$

$$\boldsymbol{\Pi} = \mathbf{g}\mathbf{S}_{\bar{v}_{\mathrm{n}}p}\tilde{\mathbf{h}}^{\mathrm{H}} \tag{17}$$

with

$$\mathbf{S}_{\bar{v}_{\mathrm{n}}\bar{v}_{\mathrm{n}}} = \langle \bar{\mathbf{v}}_{\mathrm{n}}\bar{\mathbf{v}}_{\mathrm{n}}^{\mathrm{H}} \rangle \tag{18}$$

$$\tilde{\mathbf{h}} = \mathbf{h} + \mathbf{g}\mathbf{C}_{\beta}\mathbf{C}_{\alpha} \tag{19}$$

$$\mathbf{S}_{\bar{v}_{\mathrm{n}}p} = \mathbf{G}^{-1}\tilde{\mathbf{H}}\mathbf{S}_{pp} - \mathrm{i}\omega\mathbf{T}\mathbf{S}_{up} \tag{20}$$

$$\mathbf{Q} = \mathbf{T}\mathbf{S}_{u\bar{v}_{\mathrm{n}}} = \left(\mathbf{G}^{-1}\tilde{\mathbf{H}}\mathbf{S}_{\bar{v}_{\mathrm{n}}p}^{\mathrm{H}} - \mathbf{S}_{\bar{v}_{\mathrm{n}}\bar{v}_{\mathrm{n}}}\right)/\mathrm{i}\omega \tag{21}$$

Now inserting equations (15)-(21) into equation (14), $\mathbf{S}_{pp}^{\mathrm{in}}$ can be obtained, and then the sound pressure level at the points inside the acoustic cavity can be calculated.

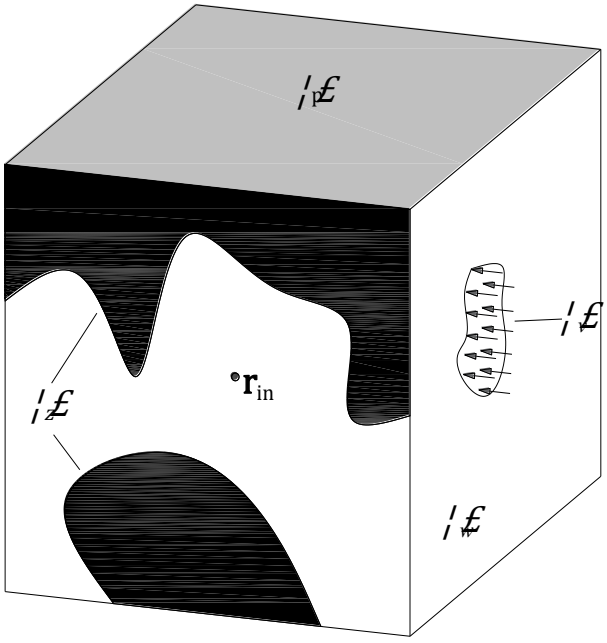


Fig. 2 A vibro-acoustic system with surface sound absorbing layer. $\Gamma_p$, a thin plate; $\Gamma_z$, the layer of sound absorbing material; $\Gamma_v$, the domain subjected to external excitation; $\Gamma_w$, the acoustically rigid walls; $\mathbf{r}_{in}$, a reference point inside the acoustic cavity.

# 3 Topology optimization problem formulation

## 3.1 Topology optimization model

Considering a vibro-acoustic system consisting of a deterministic acoustic cavity and a statistical thin plate as shown in Fig. 2, the acoustic cavity is a cuboid domain coupled with a thin plate on the upper surface. A layer of sound absorbing material is attached to the front surface of the acoustic cavity domain, and a velocity excitation is applied over a region on its right surface. The other regions of the boundary of the acoustic cavity domain are assumed to be acoustically rigid walls. By employing the hybrid BE-SEA method for the mid-frequency vibration of the vibro-acoustic system, this section

deals with the optimized layout of a given amount of sound absorbing material within a prescribed design domain for minimizing the sound pressure level at a specified point inside the cavity. The topology problem can be thus formulated as

$$\left.\begin{aligned} &\text{find} \quad \boldsymbol{\rho} = \{\rho_1 \quad \rho_2 \quad \cdots \quad \rho_{m_Z}\}^{\mathrm{T}} \\ &\min \quad \tilde{S}_{pp}^{\mathrm{in}}(\mathbf{r}_{\mathrm{in}}) = \langle p^* p \rangle \\ &\text{s.t.} \quad \sum_{k=1}^{m_Z} \rho_k V_k^0 - f_V \sum_{k=1}^{m_Z} V_k^0 \le 0 \\ &\qquad 0 < \rho_{\min} \le \rho_k \le 1 \ (k = 1, \ldots, m_Z) \end{aligned}\right\} \tag{22}$$

where $\boldsymbol{\rho}$ is the vector of the relative density design variables describing layout of the sound absorbing material. $m_Z$ represents the total number of boundary elements in the design domain, and each element has one design variable. $\tilde{S}_{pp}^{\mathrm{in}}(\mathbf{r}_{\mathrm{in}})$ represents the objective function and is a diagonal element of $\mathbf{S}_{pp}^{\mathrm{in}}$ representing the power spectral density of sound pressure (PSDSP) at a specified point $\mathbf{r}_{\mathrm{in}}$ inside the acoustic cavity. It is important to point out that the objective function can also be written as the sum of the PSDSPs at more points (i.e. $f = \sum \langle p_i^* p_i \rangle, i = 1,2 \ldots n$) to obtain an overall sound pressure reduction in the acoustic cavity (Du and Olhoff 2010). $f_V$ represents the volume fraction and $V_k^0$ is the volume of sound absorbing material in the $k$th boundary element when $\rho_k$ =1. $\rho_{\min}$ is the lower bound of the relative density variables, which is set to be $10^{-6}$ to avoid possible numerical singularity.

Based on the framework of the SIMP approach, $\mathbf{C}_\alpha$, $\mathbf{C}_\beta$ and $\mathbf{C}_\gamma$ can be respectively written as

$$\mathbf{C}_{\alpha} = \sum_{k=1}^{m_Z} (\rho_k)^N \mathbf{R}_{\alpha,Z}^{(k)} \tag{23}$$

$$\mathbf{C}_{\beta} = \mathrm{diag}\{\mathbf{E}_v - \mathbf{E}_Z\} \tag{24}$$

$$\mathbf{C}_{\gamma} = \sum_{k=1}^{m_v} \mathbf{v}_0^{(k)} \tag{25}$$

where $\mathbf{R}_{\alpha,Z}^{(k)}$ is the admittance matrix of the $k$th element of the sound absorbing layer. The penalty factor $N$ >1 is set to be $N$ =3 in this study. $\mathbf{E}_v$ and $\mathbf{E}_Z$ are location vectors corresponding to velocity and impedance boundary conditions, respectively. $\mathbf{v}_0^{(k)}$ is the velocity vector of the $k$th element of the velocity surface, and $m_v$ represents the total number of boundary elements on the velocity surface. From equations (24)-(25), it is clear that $\mathbf{C}_{\beta}$ and $\mathbf{C}_{\gamma}$ remain unchanged during the topology optimization process.

## 3.2 Sensitivity analysis

For solving the optimization model of equation (22) with a gradient-based mathematical programming algorithm, it is necessary to perform sensitivity analysis of the objective and constraint functions with respect to the design variables. The sensitivity equation for the PSDSP is derived by direct differentiation, as follows.

Differentiating the objective function in equation (22) with respect to the $k$th design variable gives $\frac{\partial \tilde{S}_{pp}^{\mathrm{in}}}{\partial \rho_k}$, a diagonal element of $\frac{\partial \mathbf{S}_{pp}^{\mathrm{in}}}{\partial \rho_k}$ which can be expressed as

$$\frac{\partial \mathbf{S}_{pp}^{\mathrm{in}}}{\partial \rho_k} = \omega^2 \left( \mathbf{g}\mathbf{T} \frac{\partial \mathbf{S}_{uu}}{\partial \rho_k} \mathbf{T}^{\mathrm{H}} \mathbf{g}^{\mathrm{H}} \right) + \mathrm{i}\omega \left[ \frac{\partial \mathbf{\Delta}}{\partial \rho_k} - \left( \frac{\partial \mathbf{\Delta}}{\partial \rho_k} \right)^{\mathrm{H}} \right] + \frac{\partial \mathbf{\Xi}}{\partial \rho_k} - \frac{\partial \mathbf{\Pi}}{\partial \rho_k} - \left( \frac{\partial \mathbf{\Pi}}{\partial \rho_k} \right)^{\mathrm{H}} \quad (26)$$

By using equations (15)-(21), $\frac{\partial \mathbf{\Delta}}{\partial \rho_k}$, $\frac{\partial \mathbf{\Xi}}{\partial \rho_k}$ and $\frac{\partial \mathbf{\Pi}}{\partial \rho_k}$ in equation (26) can be, respectively, written as

$$\frac{\partial \mathbf{\Delta}}{\partial \rho_k} = \mathbf{g} \frac{\partial \mathbf{Q}}{\partial \rho_k} \mathbf{g}^{\mathrm{H}} + \frac{\partial \tilde{\mathbf{h}}}{\partial \rho_k} \mathbf{S}_{pu} \mathbf{T}^{\mathrm{H}} \mathbf{g}^{\mathrm{H}} + \tilde{\mathbf{h}} \frac{\partial \mathbf{S}_{pu}}{\partial \rho_k} \mathbf{T}^{\mathrm{H}} \mathbf{g}^{\mathrm{H}} \quad (27)$$

$$\frac{\partial \mathbf{\Xi}}{\partial \rho_k} = \frac{\partial \tilde{\mathbf{h}}}{\partial \rho_k} \mathbf{S}_{pp} \tilde{\mathbf{h}}^{\mathrm{H}} + \tilde{\mathbf{h}} \frac{\partial \mathbf{S}_{pp}}{\partial \rho_k} \tilde{\mathbf{h}}^{\mathrm{H}} + \tilde{\mathbf{h}} \mathbf{S}_{pp} \left( \frac{\partial \tilde{\mathbf{h}}}{\partial \rho_k} \right)^{\mathrm{H}} \quad (28)$$

$$\frac{\partial \mathbf{\Pi}}{\partial \rho_k} = \mathbf{g} \frac{\partial \mathbf{S}_{\bar{v}_{\mathrm{n}} p}}{\partial \rho_k} \tilde{\mathbf{h}}^{\mathrm{H}} + \mathbf{g} \mathbf{S}_{\bar{v}_{\mathrm{n}} p} \left( \frac{\partial \tilde{\mathbf{h}}}{\partial \rho_k} \right)^{\mathrm{H}} \quad (29)$$

where

$$\frac{\partial \tilde{\mathbf{h}}}{\partial \rho_k} = \mathbf{g} \mathbf{C}_\beta \frac{\partial \mathbf{C}_\alpha}{\partial \rho_k} \quad (30)$$

$$\frac{\partial \mathbf{S}_{\bar{v}_{\mathrm{n}} p}}{\partial \rho_k} = \mathbf{G}^{-1} \frac{\partial \widetilde{\mathbf{H}}}{\partial \rho_k} \mathbf{S}_{pp} + \mathbf{G}^{-1} \widetilde{\mathbf{H}} \frac{\partial \mathbf{S}_{pp}}{\partial \rho_k} - \mathrm{i}\omega \mathbf{T} \frac{\partial \mathbf{S}_{up}}{\partial \rho_k} \quad (31)$$

$$\frac{\partial \mathbf{Q}}{\partial \rho_k} = \mathbf{T} \frac{\partial \mathbf{S}_{u \bar{v}_{\mathrm{n}}}}{\partial \rho_k} = \left( \mathbf{G}^{-1} \frac{\partial \widetilde{\mathbf{H}}}{\partial \rho_k} \mathbf{S}_{\bar{v}_{\mathrm{n}} p}^{\mathrm{H}} + \mathbf{G}^{-1} \widetilde{\mathbf{H}} \frac{\partial \mathbf{S}_{\bar{v}_{\mathrm{n}} p}^{\mathrm{H}}}{\partial \rho_k} \right) / \mathrm{i}\omega \quad (32)$$

with

$$\frac{\partial \widetilde{\mathbf{H}}}{\partial \rho_k} = \mathbf{G} \mathbf{C}_\beta \frac{\partial \mathbf{C}_\alpha}{\partial \rho_k} \quad (33)$$

Substituting equation (27)-(33) into equation (26), it can be seen that $\frac{\partial \mathbf{S}_{pp}^{\mathrm{in}}}{\partial \rho_k}$ is

determined by $\frac{\partial \mathbf{C}_\alpha}{\partial \rho_k}$ and $\frac{\partial \mathbf{S}_{qq}}{\partial \rho_k}$. Differentiating equation (23) with respect to the $k$th design variable, $\frac{\partial \mathbf{C}_\alpha}{\partial \rho_k}$ can be written as

$$\frac{\partial \mathbf{C}_\alpha}{\partial \rho_k} = \sum_{k=1}^{m} N(\rho_k)^{(N-1)} \mathbf{R}_{\alpha,Z}^{(k)} \tag{34}$$

According to equation (4), $\frac{\partial \mathbf{S}_{qq}}{\partial \rho_k}$ can be written as

$$\frac{\partial \mathbf{S}_{qq}}{\partial \rho_k} = \frac{\partial \mathbf{S}_{qq}^{\text{ext}}}{\partial \rho_k} + \frac{\partial \mathbf{S}_{qq}^{\text{rev}}}{\partial \rho_k} \tag{35}$$

where $\frac{\partial \mathbf{S}_{qq}^{\text{ext}}}{\partial \rho_k}$ and $\frac{\partial \mathbf{S}_{qq}^{\text{rev}}}{\partial \rho_k}$ can be, respectively, obtained by differentiating equations (5) and (7) with respect to the $k$th design variable and written as

$$\frac{\partial \mathbf{S}_{qq}^{\text{ext}}}{\partial \rho_k} = \boldsymbol{\chi}^{(k)} \mathbf{S}_{qq}^{\text{ext}} + \left(\boldsymbol{\chi}^{(k)} \mathbf{S}_{qq}^{\text{ext}}\right)^{\text{H}} \tag{36}$$

$$\frac{\partial \mathbf{S}_{qq}^{\text{rev}}}{\partial \rho_k} = \frac{4}{\pi \omega n_{\text{m}}} \left( E \frac{\partial \boldsymbol{\Upsilon}}{\partial \rho_k} + \frac{\partial E}{\partial \rho_k} \boldsymbol{\Upsilon} \right) \tag{37}$$

with

$$\boldsymbol{\chi}^{(k)} = -\mathbf{D}_{\text{tot}}^{-1} \frac{\partial \mathbf{D}_{\text{tot}}}{\partial \rho_k} \tag{38}$$

$$\frac{\partial \boldsymbol{\Upsilon}}{\partial \rho_k} = \boldsymbol{\chi}^{(k)} \boldsymbol{\Upsilon} + \left(\boldsymbol{\chi}^{(k)} \boldsymbol{\Upsilon}\right)^{\text{H}} \tag{39}$$

Derivatives of the thin plate energy and the total dynamic stiffness matrix with respect to the $k$th design variable respectively appear in equations (37) and (38). By using equations (2), (3) and (33), $\frac{\partial \mathbf{D}_{\text{tot}}}{\partial \rho_k}$ can be expressed as

$$\frac{\partial \mathbf{D}_{\mathrm{tot}}}{\partial \rho_k} = \begin{bmatrix} \mathbf{G}\mathbf{C}_\beta \dfrac{\partial \mathbf{C}_\alpha}{\partial \rho_k} & \mathbf{0} \\ \mathbf{0} & \mathbf{0} \end{bmatrix} \tag{40}$$

Inserting equations (36)-(40) into equation (35), it can be seen that $\frac{\partial E}{\partial \rho_k}$ is the only unknown quantity. Differentiating equation (10) with respect to the $k$th design variable, yields

$$\frac{\partial E}{\partial \rho_k} = \left( \frac{\partial P_{\mathrm{in}}^{\mathrm{dir}}}{\partial \rho_k} n_{\mathrm{m}} - \frac{\partial h_{\mathrm{out}}^{\mathrm{rev}}}{\partial \rho_k} E \right) / (h_{\mathrm{out}}^{\mathrm{rev}} + h_{\mathrm{diss}}) \tag{41}$$

By using equations (11) and (13), the partial derivative terms on the right of equation (41) can be written as

$$\frac{\partial P_{\mathrm{in}}^{\mathrm{dir}}}{\partial \rho_k} = \frac{\omega}{2} \sum_{ij} \mathrm{Im}\{\mathbf{D}_{\mathrm{dir},ij}\} \left( \frac{\partial \mathbf{S}_{uu}^{\mathrm{ext}}}{\partial \rho_k} \right)_{ij} \tag{42}$$

$$\frac{\partial h_{\mathrm{out}}^{\mathrm{rev}}}{\partial \rho_k} = \frac{2}{\pi} \mathrm{Re} \left\{ -\mathrm{i} \sum_{ij} \mathbf{C}_{\mathrm{sa},ij} \left( \frac{\partial \boldsymbol{\Upsilon}_{up}}{\partial \rho_k} \right)^*_{ij} \right\} \tag{43}$$

where $\frac{\partial \mathbf{S}_{uu}^{\mathrm{ext}}}{\partial \rho_k}$ can be obtained from equation (36).

The solution procedure for the sensitivity analysis of objective function is summarized below:

(i) The plate energy sensitivity with respect to design variables $\frac{\partial E}{\partial \rho_k}$ is obtained by inserting equations (42) and (43) into equation (41);

(ii) Substituting equation (41) into equation (37), and using equations (35) and (36), $\frac{\partial \mathbf{S}_{qq}}{\partial \rho_k}$

is then calculated;

(iii) Inserting equations (27)-(29) into equation (26), and using equations (33)-(35), one can obtain the sensitivity of the cross-spectrum matrix of sound pressure at inner points with respect to design variables $\frac{\partial \mathbf{S}_{pp}^{\text{in}}}{\partial \rho_k}$.

(iv) The objective function sensitivity with respect to design variables is calculated by using equation (26).

The sensitivity of the constraint function in the optimization model equation (22) with respect to the $k$th design variable $\rho_k$ equals $V_k^0$.

# 4 Numerical example

A simple verification example consisting of two thin plates and an acoustic cavity, as shown in Fig. 3, is presented for illustrating the validity of the proposed topology optimization model. The acoustic cavity is comprised of air and has geometrical dimensions 0.7 m by 1 m by 0.5 m. The sound speed and mass density of the air are $c_0 = 340$ m/s and $\rho_{\text{a}} = 1.225$ kg/m$^3$, respectively. Two thin plates with the same dimensions of 0.7 m by 1.0 m by 1 mm are connected respectively to the front and rear surfaces of the acoustic cavity (the gray areas in Fig. 3). The edges of the two plates are all simply supported, and the in-plane deformation of the two plates is ignored. The two plates are made of aluminum, of which the mass density, Young's modulus, Poisson's ratio and damping loss factor are 2700 kg/m$^3$, $7.1\times10^{10}$ Pa, 0.33 and 0.01, respectively.

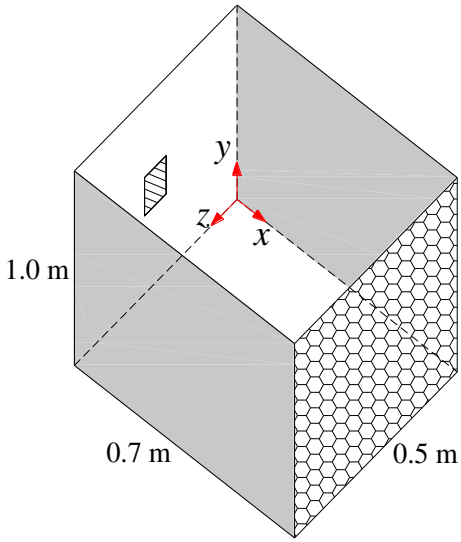


Fig. 3 Geometric diagram of the vibro-acoustic system. Diagonally hashed area, the region subjected to velocity excitation; gray area, two plates coupled to the acoustic cavity; hexagon filled area, the design domain of sound absorbing material layer; other areas, acoustically rigid walls.

The design domain of a sound absorbing layer is connected to the right surface of the acoustic cavity (the hexagon filled area in Fig. 3). A unit velocity excitation is applied over a square region (see the diagonal area in Fig. 3) of 0.04 $m^2$ on the left surface of the acoustic cavity located at the point (0, 0.5, 0.25). The other areas are considered to be acoustically rigid.

## 4.1 Response analysis for the mid-frequency vibration of the vibro-acoustic system

In order to show the efficiency of the hybrid BE-SEA method, the responses of the vibro-acoustic system calculated by employing the hybrid BE-SEA method are compared

with those calculated by using Monte Carlo simulation.

The impedance of the sound absorbing material is set to be a large real number $10^{40}$, and all element-relative densities of the sound absorbing material in the design domain are set to be 1. The frequency range considered here is from 1 Hz to 400 Hz with a frequency step of 1 Hz. Since the acoustic cavity and each thin plate respectively have 7 and 79 modes below 400 Hz, which illustrates the modal density of the acoustic cavity and each plate are significantly different, the systems will exhibit typical mid-frequency vibration behavior consisting of a deterministic acoustical behavior and a statistical structural behavior, within the frequency range of interest. In the hybrid BE-SEA model, the acoustic cavity is modeled by using the BE method, while the two plates are modeled by using SEA. A pure FE model is employed in the Monte Carlo simulation, and a regular fine FE mesh requires to be established to capture detailed deformation. Considering the influence of the uncertainties of the system, an ensemble consisting of 500 samples is generated by randomly choosing 200 points within each plate and adding 0.1% of the mass of one plate at each point.

It is important to point out that appropriate element sizes should be chosen for the parts modeled using element-based techniques in the two methods, i.e. at least six element per wavelength. Table 1 gives the details of the parts modeled using element-based techniques and the time cost by two methods. As can be seen from Table 1, the minimum number of DOFs and time cost are required for the hybrid FE-SEA method. The hybrid

implementations and the Monte Carlo simulation are performed single-threaded in Julia (v0.6.3.1) on a 3.3 GHz Intel Xeon-based system with a Windows operating system.

A comparison of the PSDSP at the point (0.3, 0.6, 0.4) inside the acoustic cavity calculated by using the hybrid BE-SEA method and the Monte Carlo simulation is shown in Fig. 4. As can be seen from Fig. 4, the resulting curves of 500 samples are concentrated at lower frequencies, which confirms that the system uncertainties have little impact on the system responses when the system is subjected to long wavelength deformation. In consideration of the sufficient uncertainty the hybrid BE-SEA has assumed over the entire frequency range, significant discrepancies can be observed between the results calculated with the two methods at lower frequencies.

Table 1 Details of two analysis models

| Analysis model | | Element type | Element size (m) | Number of elements per wavelength at 400Hz | Number of DOFs | Calculation time (h) |
|---|---|---|---|---|---|---|
| Hybrid BE-SEA | Cavity | 4-node quadrilateral | 0.050 | 17 | 1242 | 7.9 |
| | Direct field | 4-node quadrilateral | 0.025 | 6 | 1189×2 | |
| Monte Carlo simulation | Cavity | 8-node hexahedral | 0.025 | 34 | 24969 | 61.4 |
| | Plate | 4-node quadrilateral | 0.020 | 6 | 5508×2 | |

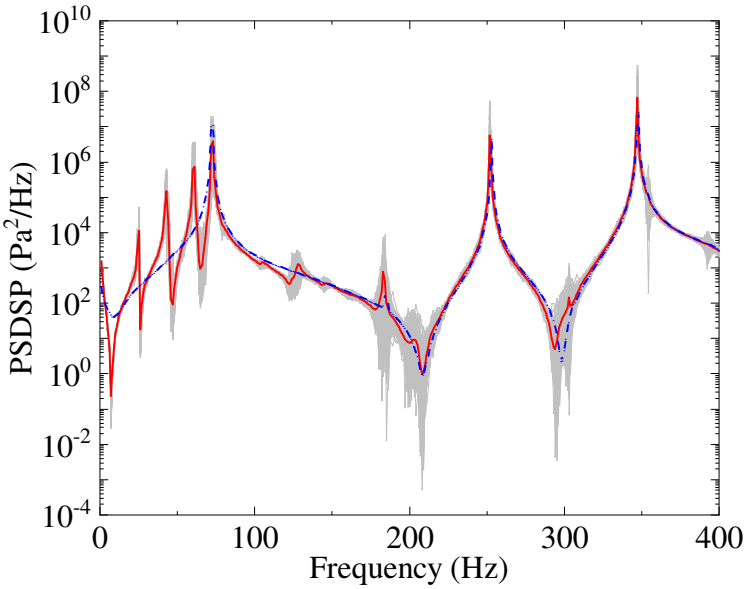


Fig. 4 PSDSP at a point inside the acoustic cavity with coordinates (0.3, 0.6, 0.4). Fine solid gray lines, computed using Monte Carlo approach for 500 realizations of ensemble; bold solid red line, ensemble average of Monte Carlo results; bold dash blue line, ensemble average computed using Hybrid BE-SEA method.

As the frequency increases, the system response becomes very sensitive to the uncertainties of the system, and the resulting curves of 500 samples become dispersed. The hybrid BE-SEA method predicts well the average trend of the pure FE method calculations with perturbed plate mass at higher frequencies. Furthermore, according to the principles of the hybrid BE-SEA method, there is sufficient uncertainty in a statistical subsystem. Hence, it should be pointed out that the average of the Monte Carlo results, which cannot involve all uncertainties (sufficient uncertainty), may have discrepancies with the results obtained by hybrid BE-SEA method even at some higher frequencies

(Cotoni et al. 2007; Shorter and Langley 2005b).

In this paper, the discrepancies at lower frequencies may be neglected since the attention is only on the mid-frequency vibration of vibro-acoustic systems.

## 4.2 Sensitivity analysis and topology optimization of sound absorbing layer for mid-frequency vibration of the vibro-acoustic system

Setting the excitation frequency to be 415 Hz, the partition of the system can be performed by wavelength analysis for the acoustic cavity and the two plates. Here, the acoustic cavity is modeled using the BE method, while the two plates are modeled using SEA. Element sizes chosen for the parts modeled using element-based techniques are the same as those in Table.1. The design domain is discretized by 200 (20×10) uniform-sized square elements. Hence there are 200 design variables $\rho_k (k = 1, 2, \ldots, 200)$. The method of moving asymptotes (MMA) (Svanberg 1987, 2002; Johnson 2008, 2014) is employed to update the design variables. The optimization process is stopped when the relative difference of the PSDSP between two adjacent iteration steps is less than $10^{-6}$.

Sensitivity analysis for the PSDSP is considered first. The point (0.35, 0.50, 0.25) is adopted as the reference point. The impedance of the sound absorbing material is set to be $Z_0 = 975+8798\mathrm{i}$ kg / ($\mathrm{m}^2$s) (see Siemens Product Lifecycle Management Software Inc 2014), and all element-relative densities of the sound absorbing material in the design domain are set to be 0.6. The relative errors of the sensitivities of the objective function

with respect to the design variables $\partial \tilde{S}_{pp}^{\text{in}}/\partial \rho_k (k = 1, 2, \ldots, 200)$, calculated by using the present method and the finite difference method (FDM) with $10^{-4}$ perturbation, are given in Fig. 5.

As can be seen from Fig. 5, the comparison shows good agreement. The FDM requires one solution of the linear system of equations for the original value plus one solution (or two if using a central perturbation method) for each design variable. For the present method, one solution of the linear system of equations for the original value is required, and then, according to section 3.2, the derivative (sensitivity) can be calculated directly by a few matrix product operations, without other solutions of the linear system of equations for each design variable. Therefore, compared with FDM, the present method requires less computation time.

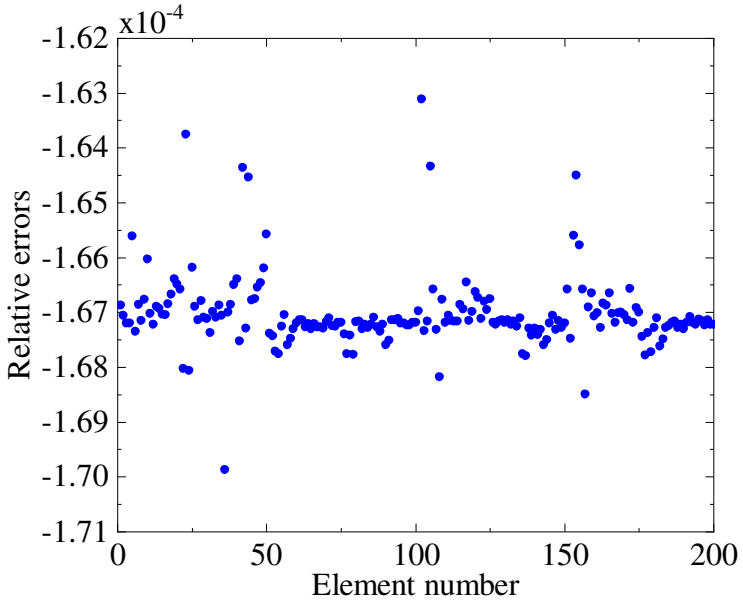


Fig.5 Relative errors of the sensitivities of the PSDSP at the reference point with respect to the element relative density of sound absorbing material.

In the following, topology optimization for the vibro-acoustic system is considered. The point (0.60, 0.50, 0.25) is adopted as the reference point. The impedance of the sound absorbing material is set as $Z_0 = 4\rho_a c_0$. All initial design variables are set to be 0.4, and the upper limit of the volume fraction of the sound absorbing material is given as $f_V = 0.5$. The optimization procedure converged after 21 iterations, and the iteration histories of the objective function and volume fraction are shown in Fig. 6. As can be seen, the PSDSP decreases significantly from 196065.61 $Pa^2/Hz$ in the initial design to 52063.696 $Pa^2/Hz$ in the final optimized design, and the volume fraction of the sound absorbing material reaches the upper limit. The sound absorbing layer layout and the contour of the PSDSP of the design domain for the initial and the optimized design are shown in Fig. 7. As can be seen, the sound absorbing material is concentrated in the places where there is a high PSDSP in the initial design, which indicates that incident sound waves reflect strongly at

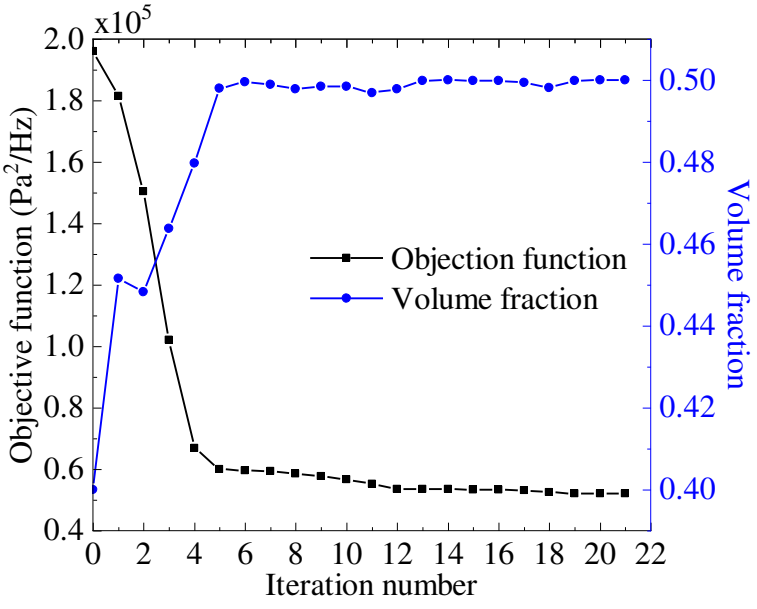


Fig. 6 Iteration histories of objective function and volume fraction.

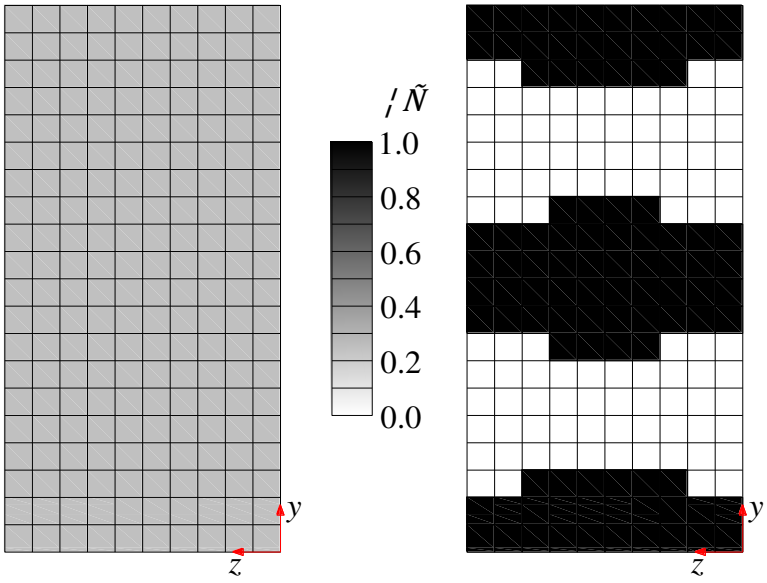


(a) Initial design (b) Optimized design

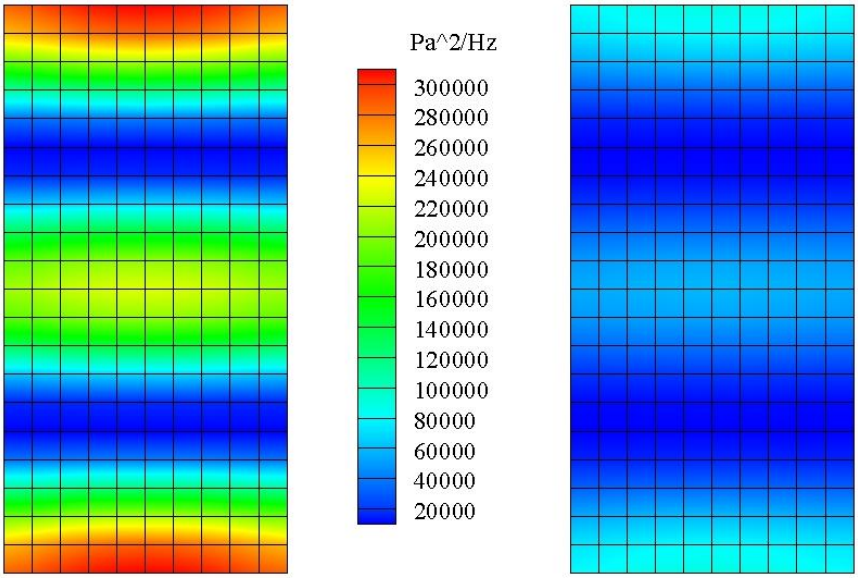


(c) Initial design (d) Optimized design

Fig. 7 Distributions of sound absorbing material for (a) the initial design, (b) the optimized design. The colorbar shows relative density of the sound absorbing material. Contours of the PSDSP for (c) the initial design, (d) the optimized design. The colorbar shows the PSDSP of the design domain.

these areas. It can be seen from Fig. 7c and d that the PSDSP of the overall design domain has significantly reduced.

Fig. 8 shows curves of PSDSP at the reference point in the frequency range of 300 Hz - 500 Hz for the initial and optimized designs. As can be seen, the natural frequencies of the system remain unchanged in the optimization process. Although the excitation frequency selected in the optimization process is 415 Hz, the PSDSP at the reference point decreases over the whole frequency range. However, it is important to point out that the dynamic optimization problem for a vibro-acoustic system is highly nonconvex. A locally optimized design is generally obtained by using a gradient-based mathematical programming algorithm, but such solutions may provide helpful guidance at the conceptual design stage.

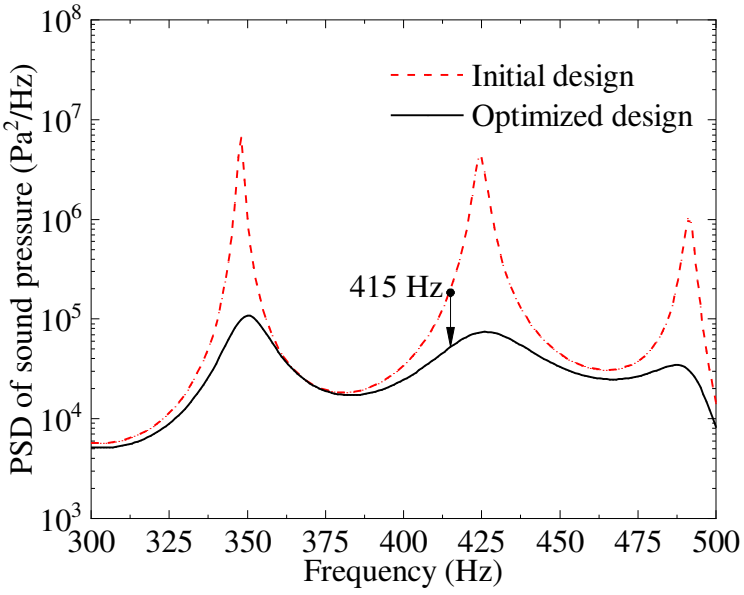


Fig. 8 Curves of PSDSP at the reference point in the frequency range of 300 Hz - 500 Hz for the initial and optimized designs.

## 4.3 Influence of excitation frequencies on optimized designs

In the following, the influence of excitation frequencies on optimized designs is considered. The point (0.60, 0.50, 0.25) is adopted as the reference point. The impedance of the sound absorbing material is set as $Z_0 = 4\rho_a c_0$. All initial design variables are set to be 0.4, and the upper limit of the volume fraction of the sound absorbing material is given as $f_V = 0.5$. The optimization process is performed by selecting the excitation frequencies as 348 Hz, 381 Hz, 425 Hz, 466 Hz, 491 Hz, 300 Hz, 400 Hz and 500 Hz. It can be seen from Fig. 8 that the first five selected frequencies correspond to the three peaks and two valleys of the curve of the PSDSP, and the last three selected frequencies correspond to the beginning, middle and end points of the frequency range of interest.

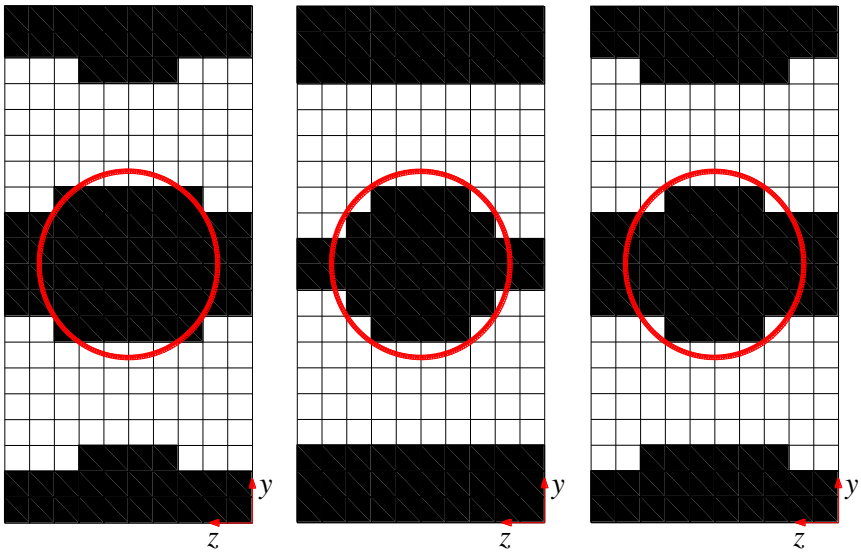


(a) 348 Hz (b) 381 Hz (c) 425 Hz

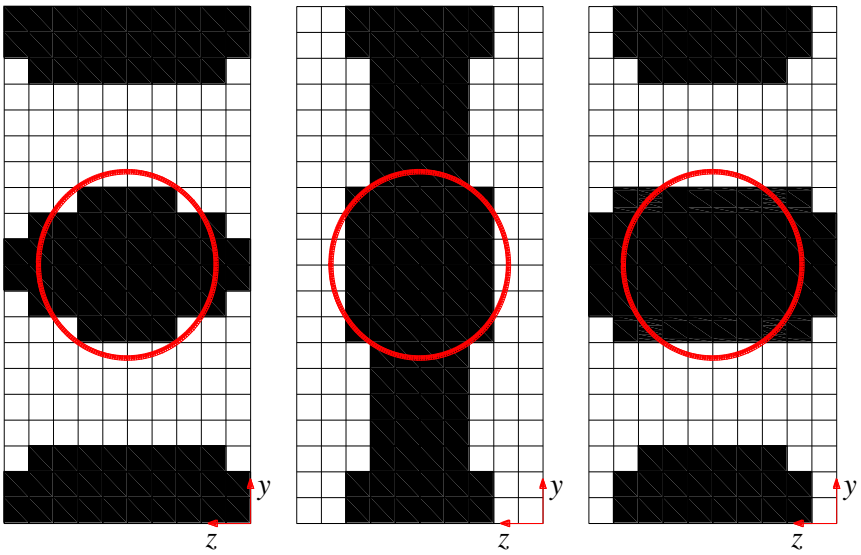


(d) 466 Hz (e) 491 Hz (f) 300 Hz

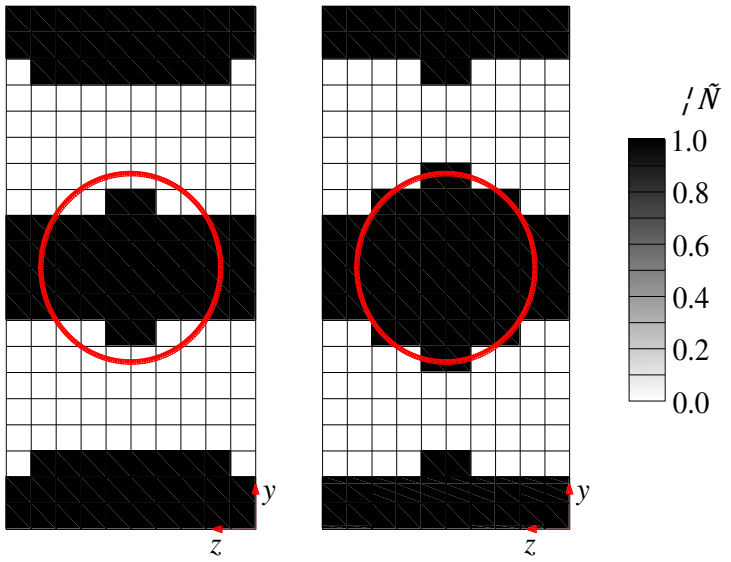


(g) 400 Hz (h) 500 Hz

Fig. 9 Optimized design under eight selected excitation frequencies. The colorbar shows relative density of the sound absorbing material.

The optimized designs obtained under each excitation frequency are shown in Fig. 9. As can be seen, the topology optimization process gives essentially the same optimized designs under most selected excitation frequencies, except for 491 Hz. Moreover, although the optimized design obtained under excitation frequency 491 Hz is obviously different from that obtained under the other seven selected excitation frequencies, the central area of the design domain (the area drawn by the red circle in Fig. 9) is always covered with sound absorbing material, which indicates that incident sound waves reflect strongly at the central area. This is natural since the direction of the velocity excitation points exactly to the central area of the design domain.

The first five optimized designs are further studied because the last three optimized designs are very similar to the first three optimized designs. The curves of PSDSP at the reference point in the frequency range of 300 Hz - 500 Hz for the initial and first five optimized designs are shown in Fig. 10. As can be seen, the PSDSP at the reference point decreases over the whole frequency range for the first five optimized designs. In addition, the five curves of PSDSP corresponding to the first five optimized designs are very close, which illustrates the importance of the central area of the design domain.

Consider now the topology optimization over the whole frequency band. Selecting 3 sampling frequencies (348 Hz, 425 Hz and 491 Hz) in the frequency band of interest, an envelope of the objection function, which is constructed by using a composite Kreisselmeier - Steinhauser objective function (Kreisselmeier and Steinhauser 1979;

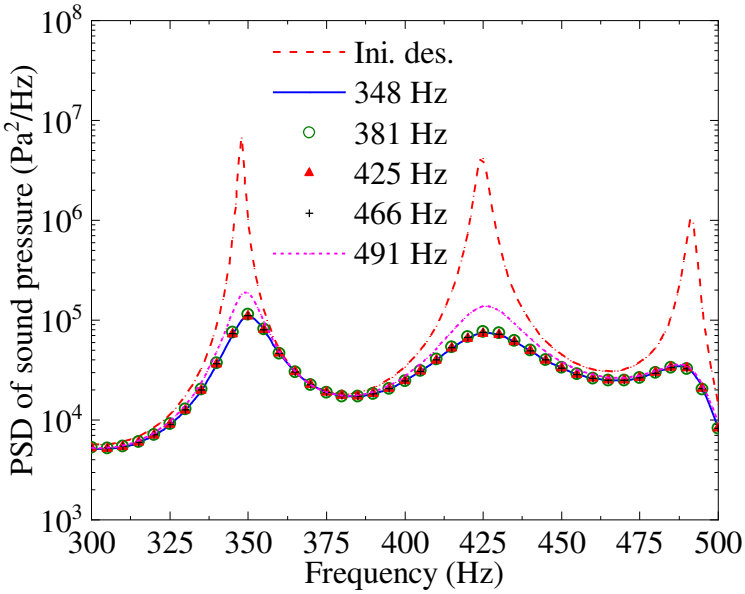


Fig. 10 Curves of PSDSP at the reference point in the frequency range of 300 Hz - 500 Hz for the initial and first five optimized designs.

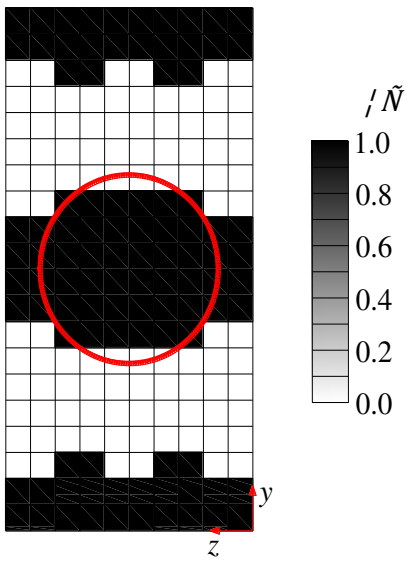


Fig. 11 Optimized design obtained using an envelope function as the objective function. The colorbar shows relative density of the sound absorbing material.

Wrenn 1989) with the aggregation parameter $\eta = 1000$, is taken as the objective function to be minimized.

The optimized design obtained using an envelope function over the whole frequency range as the objective function is shown in Fig. 11. As can be seen, it is almost the same as the optimized design obtained in Fig. 8 under 348 Hz or 425 Hz. Fig. 12 gives the comparisons between the PSDSP at the reference point in the frequency range of 300 - 500 Hz for the initial and the optimized designs. As can be seen from Fig. 12, the PSDSP at the reference point decreases over the whole frequency range for the optimized design obtained using an envelope function as the objective function. And the optimized design obtained using an envelope function, not surprisingly, gives almost the same PSDSP at the reference point as the optimized design obtained under 348 Hz or 425 Hz.

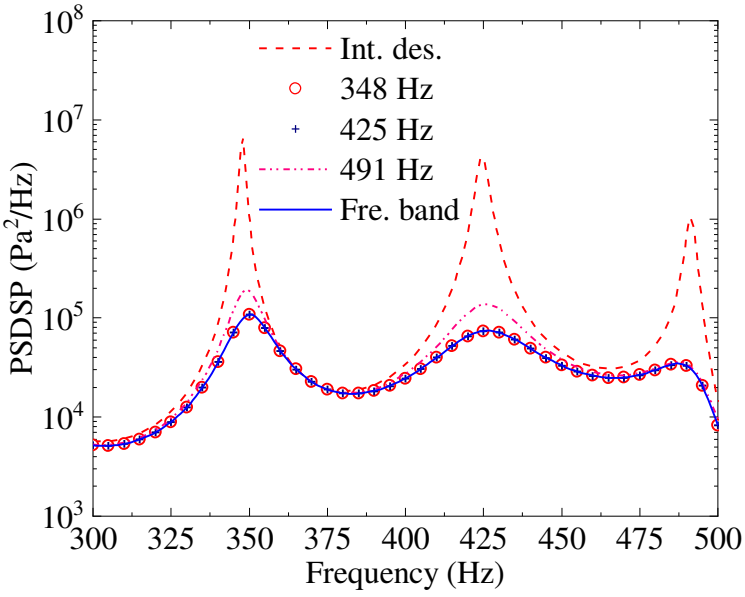


Fig. 12 Curves of PSDSP at the reference point in the frequency range of 300 - 500 Hz for the initial and optimized designs.

# 5 Conclusions

This paper performs the sensitivity analysis and topology optimization of a sound absorbing layer for minimizing the PSDSP at a specified point in the acoustic cavity when a vibro-acoustic system exhibits mid-frequency behavior. In the topology optimization model, an artificial sound absorbing material model is employed using the SIMP approach and the relative densities of the sound absorbing material are taken as design variables. The PSDSP of the acoustic cavity are calculated by using a hybrid BE-SEA method. In this context, the sensitivity analysis scheme of the PSDSP at a given reference point is developed by using the direct differentiation method. The optimized designs obtained under different excitation frequencies and using an envelope function as the objective function are also compared. The optimization process gives essentially the same optimized designs over a relatively wide frequency range. Moreover, due to the strong reflection of sound waves, the central area in the design domain which faces the region at which the velocity is applied is always covered with sound absorbing material.

# Acknowledgments

The authors are grateful for support under grants from the National Science Foundation of China (11672060), and the Cardiff University Advanced Chinese Engineering Centre.

# References


Akl W, El-Sabbagh A, Al-Mitani K, Baz A (2009) Topology optimization of a plate coupled with acoustic cavity. International Journal of Solids and Structures 46:2060-2074

Allaire G, Jouve F, Toader AM (2004) Structural optimization using sensitivity analysis and a level-set method. Journal of Computational Physics 194(1): 363-393

Bathe KJ (2008) Finite Element Method. John Wiley & Sons, Inc., Hoboken

Bendsøe MP (1989) Optimal shape design as a material distribution problem. Structural Optimization 1(4): 193-202

Bendsøe MP, Kikuchi N (1988) Generating optimal topologies in structural design using a homogenization method. Computer Methods in Applied Mechanics and Engineering 71(2): 197-224

Bendsøe MP, Sigmund O (2003) Topology Optimization, Theory, Methods and Applications. Springer, Berlin

Christensen ST, Sorokin SV, Olhoff N (1998a) On analysis and optimization in structural acoustics - Part I: Problem formulation and solution techniques. Structural Optimization 16(2-3): 83-95

Christensen ST, Sorokin SV, Olhoff N (1998b) On analysis and optimization in structural acoustics - Part II: Exemplifications for axisymmetric structures. Structural Optimization 16(2-3): 96-107

Christiansen RE, Lazarov BS, Jensen JS, Sigmund O (2015) Creating geometrically robust designs for highly sensitive problems using topology optimization. Structural and Multidisciplinary Optimization 52: 737-754

Christiansen RE, Sigmund O (2015) Experimental validation of a topology optimized acoustic cavity. Journal of the Acoustical Society of America 138: 3470-3474

Ciskowski R, Brebbia C (1991) Boundary Element Methods in Acoustics. Computational Mechanics Publications, Southampton

Cotoni V, Shorter P, Langley R (2007) Numerical and experimental validation of a hybrid finite element - statistical energy analysis method. Journal of the Acoustical Society of America 122(1): 259-270

Du J, Olhoff N (2007) Minimization of sound radiation from vibrating bi-material structures using topology optimization. Structural and Multidisciplinary Optimization 33(4-5): 305-321

Du J, Olhoff N (2010) Topological design of vibrating structures with respect to optimum sound pressure characteristics in a surrounding acoustic medium. Structural and Multidisciplinary Optimization 42(1): 43-54

Dühring MB, Jensen JS, Sigmund O (2008) Acoustic design by topology optimization. Journal of Sound and Vibration 317(3-5): 557-575

Gao R, Zhang Y, Kennedy D (2018) A hybrid boundary element-statistical energy analysis for the mid-frequency vibration of vibro-acoustic systems. Computers and

Structures 203: 34-42

Goo S, Wang S, Kook J, Koo K, Hyun J (2017) Topology optimization of bounded acoustic problems using the hybrid finite element-wave based method. Computer Methods in Applied Mechanics and Engineering 313: 834-856

Harari I, Avraham D (1997) High-order finite element methods for acoustic problems. Journal of Computational Acoustics 5(1): 33-51

Herrin DW, Martinus F, Wu TW, Seybert AF (2003) A new look at the high frequency boundary element and Rayleigh integral approximations. Society of Automotive Engineers, Technical Paper 2003-01-1451

Hinke L, Dohnal F, Mace BR, Waters TP, Ferguson NS (2009) Component mode synthesis as a framework for uncertainty analysis. Journal of Sound and Vibration 324(1-2): 161-178

Ji L, Mace BR, Pinnington RJ (2006) A mode-based approach for the mid-frequency vibration analysis of coupled long- and short-wavelength structures. Journal of Sound and Vibration 289(1-2): 148-170

Johnson SG (2008) The Nlopt nonlinear-optimization package. https://nlopt.readthedocs.io/en/latest/

Johnson SG (2014) Package to call the NLopt nonlinear-optimization library from the Julia language. https://github.com/JuliaOpt/NLopt.jl

Keane AJ, Price WG (1987) Statistical energy analysis of strongly coupled systems.

Journal of Sound and Vibration 117(2): 363-386

Kook J, Koo K, Hyun J, Jensen JS, Wang S (2012) Acoustical topology optimization for Zwicker's loudness model - Application to noise barriers. Computer Methods in Applied Mechanics and Engineering 237-240: 130-151

Kreisselmeier G, Steinhauser R (1979) Systematic control design by optimizing a vector performance index. In: IFAC symposium on computer-aided design of control systems, international federation of active controls. Zurich, Switzerland

Ladeveze P, Barbarulo A, Riou H, Kovalevsky L (2012) Mid-Frequency - CAE Methodologies for Mid-Frequency Analysis in Vibration and Acoustics. Leuven University Press, Leuven

Langley RS (1989a) A general derivation of the statistical energy analysis equations for coupled dynamic systems. Journal of Sound and Vibration 135(3): 499-508

Langley RS (1989b) Application of the dynamic stiffness method to the free and forced vibrations of aircraft panels. Journal of Sound and Vibration 135(2): 319-331

Langley RS (1992) A wave intensity technique for the analysis of high frequency vibrations. Journal of Sound and Vibration 159(3): 483-502

Lax M, Feshbach H (1947) On the radiation problem at high frequencies. Journal of the Acoustical Society of America 19(4): 682-690

Lyon RH, DeJong RG (1995) Theory and Application of Statistical Energy Analysis. 2nd ed., Butterworth-Heinemann, Boston

Ma Y, Zhang Y, Kennedy D (2015a) A hybrid wave propagation and statistical energy analysis on the mid-frequency vibration of built-up plate systems. Journal of Sound and Vibration 352: 63-79

Ma Y, Zhang Y, Kennedy D (2015b) A symplectic analytical wave based method for the wave propagation and steady state forced vibration of rectangular thin plates. Journal of Sound and Vibration 339: 196-214

Mace BR (2005) Statistical energy analysis: coupling loss factors, indirect coupling and system modes. Journal of Sound and Vibration 279(1-2): 141-170

Maxit L, Guyader JL (2003) Extension of SEA model to subsystems with non-uniform modal energy distribution. Journal of Sound and Vibration 265(2): 337-358

Muthalif AGA, Langley RS (2012) Active control of high-frequency vibration: Optimisation using the hybrid modelling method. Journal of Sound and Vibration 331(13): 2969-2983

Pluymers B, Van Hal B, Vandepitte D, Desmet W (2007) Trefftz-based methods for time-harmonic acoustics. Archives of Computational Methods in Engineering 14(4): 343-381

Shorter PJ, Langley RS (2005a) On the reciprocity relationship between direct field radiation and diffuse reverberant loading. Journal of the Acoustical Society of America 117(1): 85-95

Shorter PJ, Langley RS (2005b) Vibro-acoustic analysis of complex systems. Journal of

Sound and Vibration 288(3): 669-699

Shu L, Wang MY, Ma Z (2014) Level set based topology optimization of vibrating structures for coupled acoustic-structural dynamics. Computers and Structures 132: 34-42

Siemens Product Lifecycle Management Software Inc (2014) LMS Virtual. Lab On-line help. Munich: Siemens AG

Sigmund O (2001) A 99 line topology optimization code written in Matlab. Structural and Multidisciplinary Optimization 21(2): 120-127

Simmons C (1991) Structure-borne sound transmission through plate junctions and estimates of SEA coupling loss factors using the finite element method. Journal of Sound and Vibration 144(2): 215-227

Steel JA, Craik RJM (1994) Statistical energy analysis of structure-borne sound transmission by finite element methods. Journal of Sound and Vibration 178(4): 553-561

Svanberg K (1987) The method of moving asymptotes - a new method for structural optimization. International Journal for Numerical Methods in Engineering 24(2): 359-373

Svanberg K (2002) A class of globally convergent optimization methods based on conservative convex separable approximations. SIAM Journal on Optimization 12(2): 555-573

Van Vinckenroy G, De Wilde WP (1995) The use of Monte Carlo techniques in statistical finite element methods for the determination of the structural behaviour of composite materials structural components. Composite Structures 32(1-4): 247-253

Vergote K, Van Genechten B, Vandepitte D, Desmet W (2011) On the analysis of vibro-acoustic systems in the mid-frequency range using a hybrid deterministic - statistical approach. Computers and Structures 89(11-12): 868-877

Wang MY, Wang X, Guo D (2003) A level set method for structural topology optimization. Computer Methods in Applied Mechanics and Engineering 192(1-2): 227-246

Wrenn G (1989) An indirect method for numerical optimization using the Kreisselmeier - Steinhauser function. Contractor report NASA CR - 4220, NASA Langley Research Center, Hampton, VA, USA

Wu TW (2000) Boundary Element Acoustics: Fundamentals and Computer Codes. WIT, Southampton

Yoon GH, Jensen JS, Sigmund O (2007) Topology optimization of acoustic-structure interaction problems using a mixed finite element formulation. International Journal for Numerical Methods in Engineering 70(9): 1049-1075

Zhang X, Kang Z (2013) Topology optimization of damping layers for minimizing sound radiation of shell structures. Journal of Sound and Vibration 332(10): 2500-2519

Zhao W, Chen L, Zheng C, Liu C, Chen H (2017) Design of absorbing material distribution for sound barrier using topology optimization. Structural and

Multidisciplinary Optimization 56: 315-329

Zhao X, Vlahopoulos N (2000) Hybrid finite element formulation for mid-frequency analysis of systems with excitation applied on short members. Journal of Sound and Vibration 237(2): 181-202

Zhou M, Rozvany GIN (1991) The COC algorithm, Part II: Topological, geometry and generalized shape optimization. Computer Methods in Applied Mechanics and Engineering 89(1-3): 309-336

Zhu D, Chen H, Kong X, Zhang W (2014) A hybrid finite element-energy finite element method for mid-frequency vibrations of built-up structures under multi-distributed loadings. Journal of Sound and Vibration 333(22): 5723-5745

Zienkiewicz OC, Taylor RL (2000) The Finite Element Method. 5th ed., Butterworth-Heinemann, Oxford